Spin-Splitter and Inverse Effects in Altermagnetic Hybrid Structures

Nicolas Sigales [1,*] Tim Kokkeler [2,†] Gonzalo De Polsi [3] and Sebastian Bergeret [4,5]

[1] *Instituto de Física, Facultad de Ciencias, UdelaR, Montevideo, Uruguay*
[2] *Department of Physics and Nanoscience Center, University of Jyvaskyla, P.O. Box 35 (YFL), FI-40014 University of Jyvaskyla, Finland*
[3] *Instituto de Física, Facultad de Ciencias, UdelaR, Montevideo, Uruguay*
[4] *Centro de Física de Materiales (CFM-MPC) Centro Mixto CSIC-UPV/EHU, E-20018 Donostia-San Sebastián, Spain*
[5] *Donostia International Physics Center (DIPC), 20018 Donostia-San Sebastián, Spain*

We provide a theoretical description of diffusive charge and spin transport in hybrid devices containing altermagnets. Based on recently derived drift–diffusion equations for coupled charge and spin dynamics and general boundary conditions, our approach provides a unified description of the spin-splitter effect, i.e., the conversion of charge currents into spin currents, and its inverse in terms of experimentally accessible parameters. We analyze, analytically and numerically, the spin-splitter effect, demonstrating that an injected spin accumulation generates a measurable voltage difference across the transverse direction in the altermagnet. Motivated by a recent experiment, we also analyze a nonlocal spin-valve geometry in which an altermagnetic strip injects spin into a diffusive normal metal. We derive the resulting nonlocal voltage detected by a ferromagnetic electrode as a function of the relative orientation of the Néel vector and the ferromagnetic polarization, accounting for the main experimental findings. For this setup, we further address spin precession during diffusive transport by analyzing the spin Hanle effect. Our results provide theoretical explanations and predictions for several altermagnet hybrid structures.

I. INTRODUCTION

Since its prediction [1], altermagnetism has attracted a great deal of attention in the condensed-matter community, both theoretically [2–13], experimentally [14–19], and in connection with superconductivity [20–29]. For further references, we refer to the reviews in Refs. [30–32] and the references therein. Altermagnets (AM) are characterized by a vanishing net magnetization, as in antiferromagnets, while exhibiting a nonrelativistic spin splitting of their electronic bands, as in ferromagnets. This unique combination of properties defines a distinct class of magnetic materials that bridges the conventional distinction between ferromagnetic and antiferromagnetic order.

Beyond their fundamental interest, AM have recently emerged as a promising platform for spintronics applications, enabling the efficient generation and manipulation of spin currents without net magnetization or stray fields. In particular, the transport properties of conducting AM provide valuable insight into their microscopic magnetic structure and underlying symmetry characteristics. It was predicted in Ref. [2] that a charge current flowing through an altermagnet can generate a spin current, in a manner analogous to the spin Hall effect, but originating from the intrinsic nonrelativistic spin splitting of the altermagnetic state rather than from spin–orbit coupling. This phenomenon, known as the direct spin-splitter effect (SSE), has been supported by recent experimental observations in altermagnetic materials [16, 17].

With the exception of a few works (see, e.g., [21, 33, 34]), most theoretical studies of the SSE have focused on bulk altermagnetic materials. However, it is important to understand how this effect manifests in hybrid nanostructures, where either spin or charge currents are injected and the corresponding converted signals are detected—a standard strategy in spintronics. Examples include nonlocal spin-valve (NLSV) geometries, commonly used to measure spin currents and spin-relaxation lengths, as well as spin–orbit-based systems, where spin-to-charge conversion is detected electrically. More recently, an NLSV geometry employing an AM as a spin injector has been used with the aim to directly demonstrate the time-reversal-symmetry-breaking nature of spin injection in these materials [35]. Such transport experiments in realistic materials, *i.e.* in the presence of disorder, are most accurately described within a kinetic-equation-based approach.

In this work, we provide such a description for several setups and hybrid structures. Our analysis builds upon the drift–diffusion equations derived in Ref. [21].

* nsigales@fagro.edu.uy
† tim.h.kokkeler@jyu.fi

In Ref. [21] these equations were used to provide an illustrative demonstration of the direct spin-splitter effect in idealized configurations—such as rectangular stripes or infinite systems with perfectly transparent interfaces. More generally, previous studies of the spin-splitter effect have been restricted to bulk properties and the ballistic regime[2]. Extending such approaches to realistic hybrid structures, including spin injectors and detectors as well as unavoidable disorder, would typically require heavy numerical computations[34].

By contrast, our formulation provides a controlled and analytically tractable framework to describe diffusive transport in complex multiterminal geometries, incorporating finite interface conductance, disorder, and spin relaxation. This enables us to capture transport in terms of a reduced set of phenomenological parameters and to establish a unified description of both the direct and inverse spin-splitter effects in metallic altermagnets, as well as their connection to experimentally measurable electrical signals.

Within this framework, we analyze the spin-splitter effect, extending the results of Ref. [21] to non-ideal contacts. Additionally, we introduce the inverse spin-splitter effect, by computing the charge current or voltage induced in an altermagnet when a spin is injected. We demonstrate that, in a finite altermagnetic strip, the voltage difference induced across its edges is proportional to the total spin current injected into it. Moreover, we analyze the role of finite-size effects, interface conductance, and spin relaxation, and establish the connection between the inverse spin-splitter response and nonlocal spin-transport signals measured in multiterminal geometries.

The article is structured as follows. First, in Sec. II we discuss the theoretical framework that we use to consider transport in altermagnet hybrid structures. Then, in Sec. III we use these equations to provide a description of the spin-splitter effect in realistic systems, including disorder effects and a finite interface resistance. In Sec. IV we present the inverse of this effect, in which a transverse voltage can be generated via spin injection. Subsequently, in Sec. V we consider the setup experimentally investigated in [35] and provide expressions for the nonlocal voltage that arises in this junction. We conclude our article in Sec. VI with a summary of the main results and the conclusions we draw from them.

II. GENERALIZED KINETIC FRAMEWORK FOR CHARGE AND SPIN TRANSPORT

In this section, we briefly present the generalized kinetic framework describing the coupled transport of charge and spin in disordered systems and altermagnets. It is based on the diffusive formalism developed for collinear altermagnets in Ref. [21].

In dirty materials the electric potential μ and spin chemical potentials μ^s satisfy the following diffusion equations

$$2\nu_0\partial_t\mu + \partial_k j_k = 0\,, \tag{1}$$
$$2\nu_0\partial_t\mu^s_a + \partial_k j^s_{ka} = -2\nu_0\Gamma_{ab}\mu^s_b\,, \tag{2}$$

where ν_0 is the density of states per spin, which in altermagnets is guaranteed to be independent of spin, and Γ_{ab} is the spin–relaxation tensor [36]. In an altermagnet the spin-relaxation tensor is given by $\Gamma_{ab} = \frac{1}{\tau_s}N_aN_b + \frac{1}{\tau_{s\perp}}(\delta_{ab} - N_aN_b)$, where τ_s is the relaxation time for spin along the Néel vector $\boldsymbol{N}$ of the altermagnet and $\tau_{s\perp}$ is the relaxation time for spins perpendicular to the Néel vector. These equations describe the conservation of charge and spin densities in the diffusive regime, generalizing the framework to arbitrary dimensionality and relaxation anisotropy while allowing for a single, well-defined spin quantization axis.

The corresponding constitutive relations defining the charge, $\boldsymbol{j}$, and spin, $\boldsymbol{j}^s$ currents in altermagnets are

$$j_k = -\sigma_D\partial_k\mu - \sigma_D N_a T_{jk}\partial_j\mu^s_a\,, \tag{3}$$
$$j^s_{ka} = -\sigma_D\partial_k\mu^s_a - \sigma_D N_a T_{jk}\partial_j\mu - \sigma_D N_b K_{jk}\epsilon_{abc}\partial_j\mu^s_c\,. \tag{4}$$

with $\sigma_D = 2D\nu_0$ the Drude conductivity, D the diffusion coefficient, and ν_0 the density of states per spin at the Fermi level.

The tensors T_{jk} and K_{jk} encode the spin–momentum coupling intrinsic to altermagnets: T_{jk} represents the linear coupling between charge and spin gradients allowed by the underlying crystal symmetry, whereas K_{jk} describes the interconversion between spin currents with spin polarizations perpendicular to the Néel vector, analogous to the spin-swapping effect [37] in systems with spin–orbit coupling.

The general boundary conditions that complement Eqs. (1)–(4) and govern transport across hybrid interfaces take the compact

$$\begin{pmatrix}\hat{n}\cdot j_e\\ \hat{n}\cdot j^s_a\end{pmatrix} = -G_B\begin{pmatrix}\mu_{\rm res}-\mu\\ m_a\mu^s_{\rm res}-\mu^s_a\end{pmatrix} - PG_B\begin{pmatrix}\mu^s_{\rm res}-\boldsymbol{\mu}^s\cdot\boldsymbol{m}\\ m_a(\mu_{\rm res}-\mu)\end{pmatrix}\,, \tag{5}$$

where $G_B = G_\uparrow + G_\downarrow$ is the total barrier conductance per unit area, and $P = (G_\uparrow - G_\downarrow)/(G_\uparrow + G_\downarrow)$. Here, $\uparrow$ and $\downarrow$ refer to the spin polarization of the barrier itself, or to the spin quantization axis, $\boldsymbol{m}$ if a ferromagnet is one of the junction electrodes.

Eqs. (3)-(5) establish the main equations for analyzing spin–charge conversion phenomena, such as the spin-splitter effect (SSE) and its inverse, discussed in the following sections.

Throughout this article, we consider collinear AMs, in which the Néel vector $\boldsymbol{N}$ is homogeneous. In this case, the spin accumulation is aligned with $\boldsymbol{N}$, and the spin chemical potential can be written as $\mu^s_a = N_a\mu^s$. Since the $\tau_{s\perp}$ and K_{jk} terms only affect spin components perpendicular to the Néel vector, they do

not contribute to the transport equations in this collinear regime. Thus, we may write a single spin relaxation time τ_s. This situation corresponds to the case relevant for monodomain d–wave altermagnets. In this collinear regime, the spin-current tensor reduces to a single component $j_k^s \equiv N_a j_{ka}^s$.

Thus, in this case, Eqs. (3-4) for the charge and spin currents reduce to

$$\begin{cases} j_k = -\sigma_D \left(\partial_k \mu + T_{kj}\partial_j \mu^s\right) , \\ j_k^s = -\sigma_D \left(\partial_k \mu^s + T_{jk}\partial_j \mu\right) . \end{cases} \tag{6}$$

In the remaining sections we will use the above equations and boundary conditions to describe the spin-splitter effect, III, its inverse, IV, and transport in a non-local spin valve V. To maximize the spin–charge interconversion, we choose the orientation of the d-wave "flower"

as shown in Figs. 1 and 3. Generalization to other orientations is straightforward and will not be considered here.

III. THE SPIN–SPLITTER EFFECT IN AN ALTERMAGNETIC STRIP

In this section we analyze the spin–splitter effect in a diffusive altermagnetic strip. Starting from the constitutive relations for charge and spin currents, we formulate the model describing how the spin–momentum coupling intrinsic to the altermagnet gives rise to coupled spin and charge transport under an applied electric bias. With this, we generalize the results obtained in [21] for a perfect contact between the altermagnet and the electrode to the more realistic setting in which there is a finite barrier resistance. We consider three geometries, illustrated in Fig. 1: a transverse voltage bias in an infinite strip (a), a longitudinal electric field configuration (b), and a finite rectangular sample (c).

A. Altermagnetic strip with a transverse voltage

We first consider the configuration shown in Fig. 1(a): a two-dimensional altermagnetic (AM) strip infinite along the x direction and of finite width L_y along y. A transverse voltage $\pm V/2$ is applied at the edges $y = \pm L_y/2$.

At the AM/normal-metal interfaces, the boundary conditions for the charge current follow from Eq. (5) and read

$$\sigma_D n_y \partial_y \mu = G_B \left(\mu_{\rm res} - \mu\right) . \tag{7}$$

Due to translational invariance along x, both the electrochemical potential μ and the spin accumulation μ^s depend only on the transverse coordinate y. Solving for $\mu(y)$ yields

$$\mu(y) = \frac{G_B V}{G_B L_y + 2\sigma_D}\, y . \tag{8}$$

The corresponding charge current is

$$j_y = -\frac{G_B(\sigma_D/L_y)}{G_B + 2(\sigma_D/L_y)}\, V , \tag{9}$$

which reflects a series combination of the two interface conductances G_B and the transverse conductance of the altermagnet σ_D/L_y. At this order, the spin accumulation vanishes, $\mu^s = 0$.

According to Eq. (6), a charge current induces a spin current via the spin-splitter effect,

$$j_x^s = T_{xy}\, j_y . \tag{10}$$

In the limit of large interface conductance, $G_B \gg \sigma_D/L_y$, this expression reduces to

$$j_x^s = -\sigma_D T_{xy}\, \frac{V}{L_y} , \tag{11}$$

in agreement with Ref. [21].

B. Longitudinal voltage

We now consider a finite AM with rectangular geometry of length L_x and width L_y, as shown in Fig. 1(c). The altermagnet is connected at $x = 0$ and $x = L_x$ to two normal-metal reservoirs biased at voltages $\pm V/2$. The transverse boundaries at $y = \pm L_y/2$ are assumed to be insulating for both charge and spin currents.

Charge and spin transport within the altermagnet are described by the electrochemical potential $\mu(x, y)$ and the spin accumulation $\mu^s(x, y)$. Using the drift–diffusion framework introduced previously, Eqs. (1)–(6), the coupled diffusion equations take the form

$$(\partial_x^2 + \partial_y^2)\mu + 2T_{xy}\partial_x\partial_y\mu^s = 0 , \tag{12}$$

$$(\partial_x^2 + \partial_y^2)\mu^s + 2T_{xy}\partial_x\partial_y\mu = \frac{\mu^s}{\ell_s^2} . \tag{13}$$

In the following, we treat the spin–charge coupling parameter T_{xy} perturbatively and retain only terms up to linear order in T_{xy}.

At the interfaces with the electrodes, $x = 0,\ L_x$, the boundary conditions follow from Eq. (5). For the charge sector, they read

$$\sigma_D n_x \partial_x \mu = G_B(\mu_{\rm res} - \mu) , \qquad x = 0, L_x , \tag{14}$$

whereas for the spin sector (the normal-metal reservoirs are assumed not to sustain any spin accumulation, $\mu^s_{\rm res} = 0$) Eq. (5) yields

$$\sigma_D\, n_x \partial_x \mu^s = -G_B\, \mu^s , \qquad x = 0, L_x , \tag{15}$$

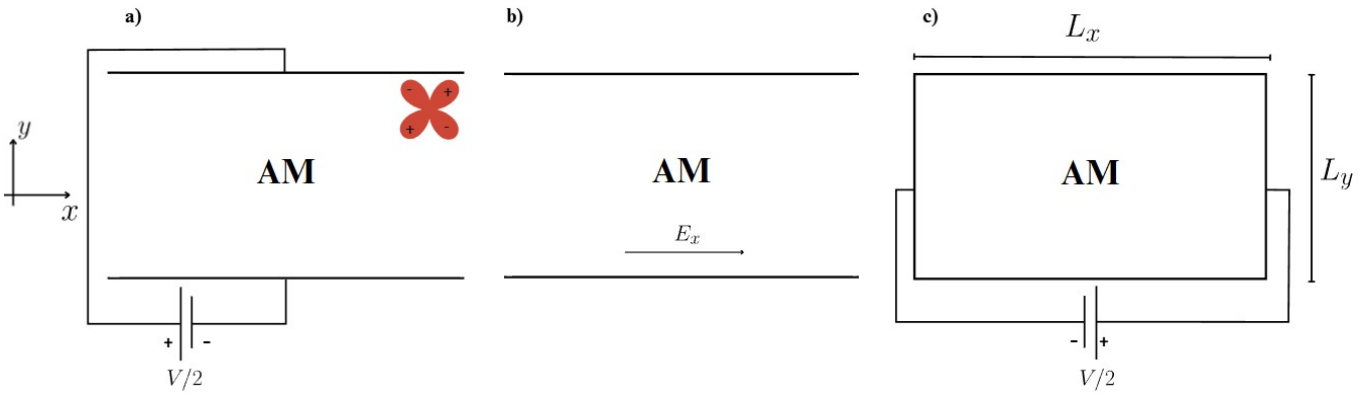

Figure 1. Model geometries considered for the spin–splitter effect in an altermagnetic (AM) strip. (a) Transverse voltage bias configuration, where electrochemical potentials $\pm V/2$ are applied at the edges $y = \pm\frac{L_y}{2}$. (b) Longitudinal electric field configuration, with a uniform field E_x applied along the strip axis. (c) Finite rectangular geometry of dimensions $L_x \times L_y$, combining a transverse voltage bias and open lateral boundaries. These configurations serve as the basis for modeling spin–charge coupling in diffusive altermagnets.

where n_x denotes the outward normal to the altermagnet. At the transverse boundaries $y = \pm L_y/2$, the y-components of both charge and spin currents vanish.

To solve the resulting boundary-value problem, we proceed perturbatively in T_{xy}. At zeroth order, the electrochemical potential follows from the diffusion equation, Eq. (12), which together with the interface boundary conditions, Eq. (14), with $\mu_{\rm res} = \pm V/2$ results in

$$\mu(x) = \frac{G_B}{G_B L_x + 2\sigma_D}\left(x - \frac{L_x}{2}\right) V \,. \tag{16}$$

For highly transparent interfaces, $G_B \gg \sigma_D/L_x$, this expression reduces to $\mu = V(x - L_x/2)/L_x$.

According to the previous section, the finite longitudinal gradient of μ induces a transverse spin current via the spin-splitter effect. At $y = \pm L_y/2$ we impose vanishing spin current, which according to Eq. (5) leads to the following B.C.:

$$\partial_y \mu^s|_{y=\pm L_y/2} = -\,T_{xy}\,\frac{G_B V}{G_B L_x + 2\,\sigma_D} \,. \tag{17}$$

Up to linear order in T_{xy}, the spin accumulation obeys the diffusion equation Eq. (13)

$$(\partial_x^2 + \partial_y^2)\mu^s = \frac{\mu^s}{\ell_s^2} \,, \tag{18}$$

subject to the boundary conditions, Eqs. (15,17).

The resulting spin accumulation can be written in closed form as

$$\mu^s(x,y) = -\,T_{xy}\,\frac{V\ell_s}{L_x + 2\sigma_D/G_B}\left(\frac{\sinh\frac{y}{\ell_s}}{\cosh\frac{L_y}{2\ell_s}} + \frac{4}{L_y\ell_s}\sum_{m=0}^{\infty}\frac{1}{k_m^2}\right.$$
$$\left.\frac{G_B}{\sigma_D k_m \sinh\!\left(k_m\frac{L_x}{2}\right) + G_B\cosh\!\left(k_m\frac{L_x}{2}\right)}\cosh\left[k_m\left(x - \frac{L_x}{2}\right)\right]\cos\left[\frac{(2m+1)\pi}{L_y}\left(y + \frac{L_y}{2}\right)\right]\right) \,, \tag{19}$$

where

$$k_m^2 = \ell_s^{-2} + \frac{(2m+1)^2\pi^2}{L_y^2} \,. \tag{20}$$

Equation (19) corresponds to a Fourier mode expansion that automatically satisfies the transverse boundary conditions. The corresponding spatial spin profile is shown in Fig. 2, illustrating the distribution of the spin in the finite AM.

One can verify that in the limit of perfectly transparent interfaces, $G_B \to \infty$, Eq. (19) coincides with the result presented in Ref. [21].

Another limiting case is the infinite strip in the x direction, Fig. 1(b). Because of translational invariance along x, the spin accumulation depends only on y, and it is given by the first term in parentheses in Eq. (19):

$$\mu^s(y) = -\,T_{xy}\ell_s\,E_x\,\frac{\sinh(y/\ell_s)}{\cosh(L_y/2\ell_s)} \,, \tag{21}$$

where E_x is the homogeneous electric field along the strip, see Fig. 1(b). The spin accumulation at the edges follows directly from Eq. (21) and is given by

$$\mu^s\left(\pm\frac{L_y}{2}\right) = \pm T_{xy}\ell_s\, E_x\, \tanh\left(\frac{L_y}{2\ell_s}\right) . \tag{22}$$

This spin accumulation can be detected directly using magnetic electrodes and non-local spin-valve measurements, as discussed in Sec. V, or indirectly via SMR-type measurements [17, 38].

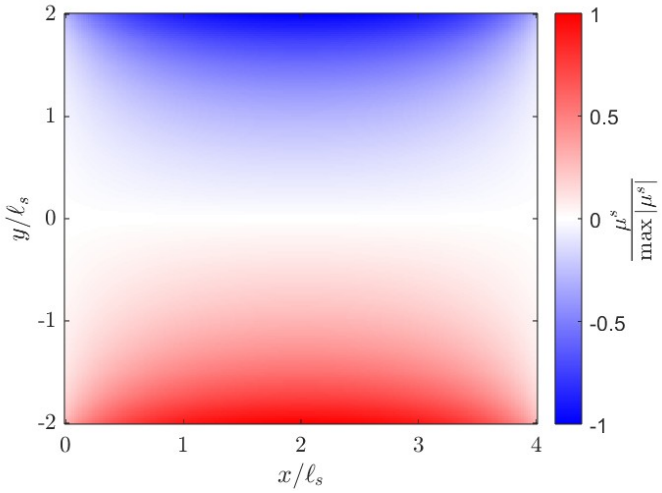

Figure 2. Spin accumulation in a finite altermagnetic strip induced by a longitudinal voltage difference, see Fig. 1(c). The dimensions of the strip are $L_x/\ell_s = L_y/\ell_s = 4$. The plot is obtained from Eq. (19) for $G_B\ell_s/\sigma_D = 1.5$, illustrating the spatial profile of the spin accumulation.

IV. THE INVERSE SPIN-SPLITTER EFFECT

Following Eq. (6), the tensor T_{jk} enters the expressions for the charge current and spin current analogously. This suggests that the spin-splitter effect discussed in the previous section, in which a voltage generates a spin accumulation, should be accompanied by a reciprocal response, the generation of a charge accumulation via a spin voltage, which we term the inverse spin-splitter effect.

In this section we analyze the inverse spin–splitter effect in a diffusive altermagnetic strip.

We consider three spin-injection geometries, illustrated in Fig. 3: a uniform spin accumulation applied to an infinite strip (a), spin injection into a finite strip (b), and a local spin injection in a finite sample (c).

A. Infinite altermagnetic strip

We first consider an altermagnetic strip that is infinite along the x–direction and has a finite width L_y along y, as illustrated in Fig. 3(a). This configuration is reciprocal to the one studied in Sec. III: instead of applying an electric bias, a transverse *spin accumulation* (or spin voltage) is imposed at $y = L_y/2$, while charge transport across the boundaries is suppressed. Such a situation can be realized, for instance, by spin pumping, or in nonlocal spin–valve geometries where a pure spin current is injected into the altermagnet.

Because the system is translationally invariant in the x-direction, μ^s depends only on y, satisfying, in the stationary regime, the spin diffusion equation

$$\partial_y^2\mu^s = \frac{\mu^s}{\ell_s^2} . \tag{23}$$

At the upper edge, see Fig. 3(a), $y = L_y/2$, the boundary condition, Eq. (5), reads

$$\sigma_D n_y \partial_y\mu^s = G_B\big(V_s - \mu^s\big)\big|_{y=\frac{L_y}{2}} , \tag{24}$$

whereas at $y = -L_y/2$ we impose a zero spin current, *i.e.* $\partial_y\mu^s = 0$.

The solution of Eq. (23) together with these boundary conditions is given by

$$\mu_s(y) = \frac{V_s}{1+\dfrac{\sigma_D}{G_B\ell_s}\tanh\left(\dfrac{L_y}{\ell_s}\right)}\,\frac{\cosh\left(\dfrac{y+L_y/2}{\ell_s}\right)}{\cosh\left(\dfrac{L_y}{\ell_s}\right)} . \tag{25}$$

According to Eq. (6), the spin current, proportional to the spin gradient leads to a longitudinal charge current via the inverse spin-splitter effect:

$$j_x = -\sigma_D T_{xy}\partial_y\mu^s . \tag{26}$$

Substitution of Eq. (25), leads to

$$j_x(y) = -\frac{\sigma_D T_{xy}V_s}{\ell_s}\,\frac{\sinh\left(\dfrac{y+L_y/2}{\ell_s}\right)}{\left[1+\dfrac{\sigma_D}{G_B\ell_s}\tanh\left(\dfrac{L_y}{\ell_s}\right)\right]\cosh\left(\dfrac{L_y}{\ell_s}\right)} . \tag{27}$$

The total longitudinal charge current induced by the imposed spin accumulation is obtained by integration over y:

$$I_{\rm ISS} = -\frac{\sigma_D T_{xy}V_s}{1+\dfrac{\sigma_D}{G_B\ell_s}\tanh\left(\frac{L_y}{\ell_s}\right)}\,\frac{\cosh\left(\frac{L_y}{\ell_s}\right)-1}{\cosh\left(\frac{L_y}{\ell_s}\right)} . \tag{28}$$

In the limit of large interface conductance, $G_B \gg \sigma_D/\ell_s$, Eq. (28) simplifies to

$$I_{\rm ISS} = -G_B\ell_s T_{xy}\frac{\cosh\left(\frac{L_y}{\ell_s}\right)-1}{\sinh\left(\frac{L_y}{\ell_s}\right)} \tag{29}$$

Let us now assume that the stripe is also finite in the x direction, as shown in Fig. 3(b). In this case the total

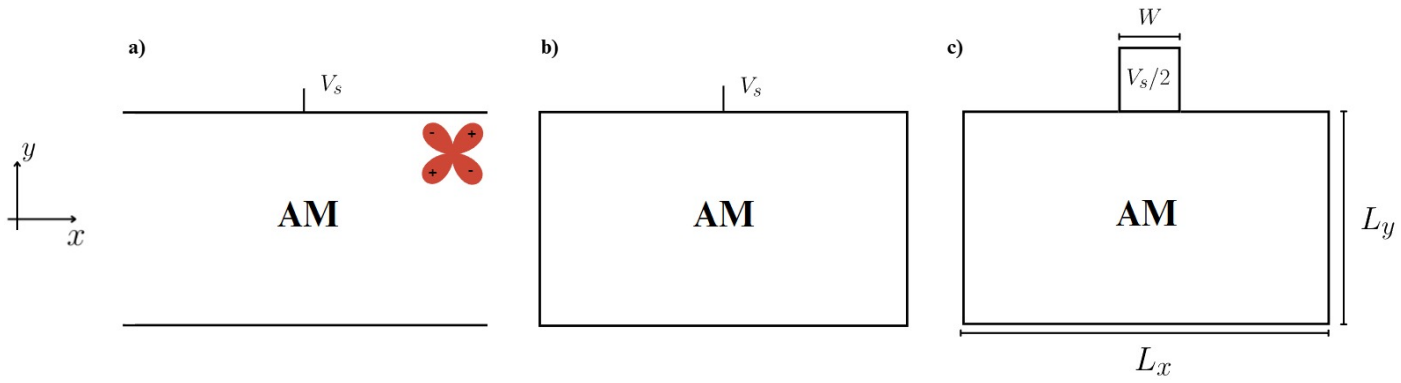

Figure 3. Geometries considered for transverse spin injection in an altermagnetic (AM) strip. (a) Uniform spin injection at the upper transverse boundary of an infinite strip, assuming translational invariance along the longitudinal direction. (b) Spin injection at the upper transverse edge of a finite strip, with transverse boundaries located at $y = \pm L_y/2$. (c) Spin injection localized over a finite region of the upper transverse edge of a finite strip.

average current is zero, $I_x = \int dy j_x = 0$. Hence, from Eq. (6) we obtain:

$$\frac{1}{L_y}\int dy \partial_x \mu = -\frac{T_{xy}}{L_y}\Delta\mu^s \,, \tag{30}$$

where $\Delta\mu^s$ is the difference of the spin in the upper and lower edges. If we now integrate this equation with respect to x we obtain the average voltage between the transverse edges. Up to linear order in T_{xy}, we can use the solution Eq. (25) for μ_s resulting in:

$$V_{\rm ISS} = -\frac{T_{xy}L_x}{L_y}\frac{V_s}{1+\dfrac{\sigma_D}{G_B\ell_s}\tanh\left(\dfrac{L_y}{\ell_s}\right)}\frac{\cosh\frac{L_y}{\ell_s}-1}{\cosh\frac{L_y}{\ell_s}} \,. \tag{31}$$

This is the transverse voltage generated by spin injection in an open geometry. As expected, this corresponds to the expression for the transverse current $I_{\rm ISS}$, Eq. (28), divided by the effective transverse conductance, $\sigma_D L_y/L_x$.

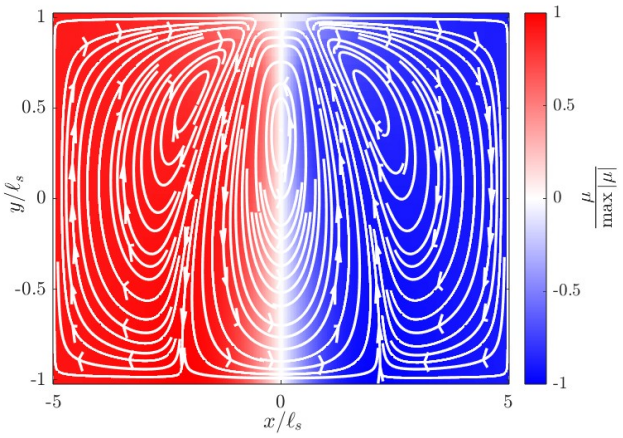

Figure 4. Normalized electrochemical potential $\mu(x,y)/\max|\mu|$ together with the induced charge current streamlines generated by localized Gaussian spin injection at the upper edge of a finite altermagnetic strip. Spatial coordinates are given in units of the spin relaxation length ℓ_s. The parameters used are $L_x/\ell_s = 10$, $L_y/\ell_s = 2$ and a Gaussian injection profile of width $W = 0.25\,\ell_s$ centered at $x = 0$.

B. Local spin injection in an altermagnetic strip

Thus far we have only considered geometries in which the contact between the injector and the altermagnet is wide, extending along the whole edge. Another geometry that can be realized is that of a local injector. To study this type of system, we consider the configuration illustrated in Fig. 3(c).

Charge and spin transport in the altermagnet are governed by the same drift–diffusion equations introduced in the previous sections Eqs. (12) and (13), together with the constitutive relations of the model Eqs. (6) and (5). In the present geometry, the essential new ingredient is the localized character of the spin injection, which enters through the boundary conditions at the upper transverse edge of the strip.

We consider spin injection through an injector of width W, implemented with a Gaussian profile of the interface conductance [1], satisfying $W \ll \ell_s, L_x, L_y$. In this regime, the injector can be approximated as point-like and is described by a Dirac δ-function in the boundary conditions.

The boundary conditions along the transverse

[1] Implementing the local injector with a Gaussian profile improves the numerical stability, but does not affect the physics, as we confirm by shrinking its width.

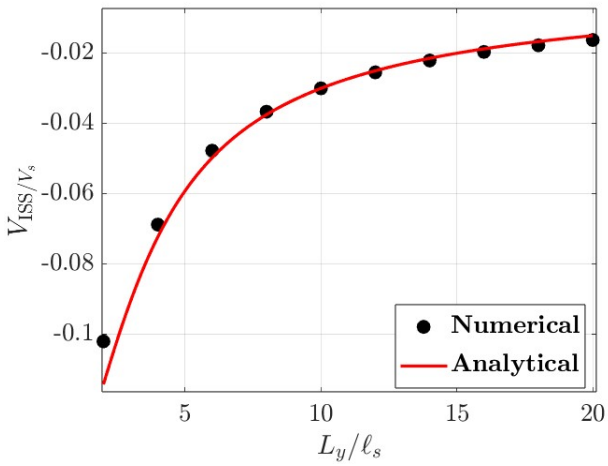

Figure 5. Induced inverse spin–splitter voltage $V_{\rm ISS}$ as a function of the transverse strip length L_y. Symbols correspond to the numerical results obtained from the full diffusive calculation, while the solid line shows the semi–analytical prediction given by Eq. (35). Parameters used are $G_B W/\sigma_D = 0.15$, $T_{xy} = 1$, and $L_x/\ell_s = 40$.

direction read

$$\partial_y \mu_s^z + T_{xy}\partial_x \mu\big|_{x,y=-L_y/2} = 0 \,, \tag{32}$$

$$\sigma_D(\partial_y \mu_s^z + T_{xy}\partial_x \mu)\,|_{x,y=L_y/2} = G_B\, W\, \delta(x)\big(V_s - \mu_s^z(x, \frac{L_y}{2})\big) \,. \tag{33}$$

Here, W is the effective width of the injector and V_s is the applied spin voltage. The Dirac delta explicitly encodes the localized nature of the injection, while the term proportional to μ_s^z accounts for the back-action of the induced spin accumulation at the interface.

At $x = \pm\frac{L_x}{2}$, we impose vanishing currents normal to the interface,

$$\partial_x \mu_s^z(\pm\frac{L_x}{2}, y) + T_{xy}\partial_y \mu(\pm\frac{L_x}{2}, y) = 0 \,. \tag{34}$$

Although a closed analytical solution for the full spatial profiles $\mu(x, y)$ and $\mu_s^z(x, y)$ is not available, an analytical expression for the ISS-induced voltage along the x-direction can be obtained by focusing on the spin accumulation averaged over the entire sample area. As shown in Appendix A 2, the induced voltage can be written as

$$V_{\rm ISS} = -T_{xy}\,\frac{L_x}{\ell_s}\,\langle \mu_s \rangle\, \tanh\!\left(\frac{L_y}{2\ell_s}\right) \,, \tag{35}$$

where $\langle \mu_s \rangle$ denotes the spin potential averaged over the full two-dimensional geometry of the altermagnetic strip.

To evaluate $\langle \mu_s \rangle$, we integrate the diffusion equation for μ_s^z over the entire spatial domain and make use of the boundary conditions Eqs. (32) and (33). This yields, to lowest order in T_{xy} (see Appendix A 1 for details),

$$\langle \mu_s \rangle = \frac{G_B\, W \ell_s^2}{\sigma_D L_x L_y}\big(V_s - \mu_s^z(0, \frac{L_y}{2})\big) \,. \tag{36}$$

Let us consider the case in which the interface conductance is small $G_B W \ll \sigma_D$. Since μ_s vanishes in the absence of the electrode, the term $G_B W \mu_s^z(0, \frac{L_y}{2})$ contributes only at order $\mathcal{O}((G_B W/\sigma_D)^2)$ in Eq. (36) and can therefore be neglected at leading order. With this, Eq. (36) reduces to (see Appendix A 1 for details)

$$\langle \mu_s \rangle \approx \frac{2G_B\, W \ell_s^2}{\sigma_D L_x L_y}\, V_s \,. \tag{37}$$

Together with Eq. (35), this provides a closed-form expression for $V_{\rm ISS}$ in the weak-coupling regime.

To validate the analytical result and characterize the full spatial response, Eqs. (12) and (13) are solved numerically together with the boundary conditions Eqs. (32) and (33). The numerical solutions yield the stationary profiles of $\mu(x, y)$ and $\mu_s^z(x, y)$, from which the induced charge current density is reconstructed.

Figure 4 shows the electrochemical potential $\mu(x, y)$ together with the corresponding charge current streamlines. Three distinct current loops emerge as a consequence of the anisotropic transport tensor of the altermagnet combined with the localized nature of the spin injection, providing a clear manifestation of the inverse spin–splitter mechanism. Such current loops have also been obtained in Ref. [34] in other setups, for which the authors claim they can be measured using magnetometry techniques. Here, in contrast, we focus on electric measurements of the transverse electrical signals in conventional transport experiments using multiterminal devices.

The inverse spin–splitter voltage is obtained from the numerical solution as the difference between the electrochemical potentials averaged over the transverse direction at the two lateral edges of the strip. The resulting $V_{\rm ISS}$ is shown in Fig. 5 as a function of the transverse length L_y. Symbols correspond to the numerical results, while the solid line represents the analytical prediction derived within the first-order expansion in the barrier conductance G_B in Eqs. (35) and (37). The agreement demonstrates that the leading-order analytical treatment accurately captures the essential features of the inverse spin–splitter effect induced by point-like spin injection.

In short, the results presented in this section establish the inverse spin–splitter effect as the reciprocal counterpart of the spin–splitter effect discussed in Sec. III. In both cases, the conversion mechanism is governed by the same nonrelativistic spin–momentum coupling intrinsic to the altermagnetic state and does not rely on (relativistic) spin–orbit interaction. The analytical and numerical results obtained for extended and localized spin injection geometries demonstrate

that the inverse response is robust against details of the injection profile and interface transparency, providing a consistent and experimentally accessible signature of altermagnetic spin–charge conversion in hybrid nanostructures.

V. HYBRID MULTI-TERMINAL SETUPS

In the previous sections, we analyzed how charge–spin interconversion arises in altermagnets within a generalized drift–diffusion framework. In this section, motivated by the recent non-local spin-valve experiment reported in Ref. [35], we study how this conversion manifests itself in hybrid multi-terminal transport geometries. In particular, we show that a charge current flowing along an altermagnetic strip generates a non-local electrical signal in an attached normal metal through spin injection mediated by the spin–splitter effect. The magnitude and sign of the resulting non-local voltage are controlled by the orientation of the Néel vector, establishing a direct connection between altermagnetic order and non-local spin transport.

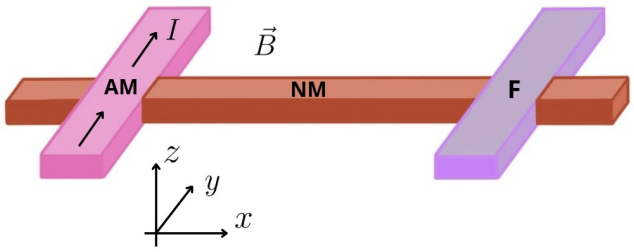

Figure 6. Hybrid nonlocal spin valve. A finite altermagnetic strip injects spin into a diffusive normal metal, which is electrically detected by a ferromagnetic (F) electrode. The induced spin can be rotated by an external magnetic field $\boldsymbol{B}$.

We consider a typical non-local spin valve [39–41] shown in Fig. 6, consisting of a diffusive normal metal (NM) attached to an altermagnetic strip and a ferromagnetic detector. In the configuration considered here, the driving charge current flows exclusively along the altermagnetic arm, while the normal metal and ferromagnetic electrodes act solely as spin transport and detection elements. When a charge current flows along the AM arm, a transverse spin current is generated via the spin–splitter effect discussed in Section III. This spin current is injected into the NM and diffuses over the spin diffusion length, which in metals such as Cu can reach micrometer scales. The resulting spin accumulation is detected electrically by a ferromagnetic electrode placed at a distance from the injector. The geometry corresponds to the one of the electrical bias geometry of a recent experiment reported in Ref. [35]. In what follows, we compute the resulting non-local voltage signal. In addition to the zero-field configuration, we also consider an external magnetic field applied along the NM wire, which induces spin precession and gives rise to a Hanle-type response.

In the stationary diffusive regime, spin transport in the NM is governed by

$$\partial_x^2 \boldsymbol{\mu}^s - \frac{\boldsymbol{\mu}^s}{\ell_{NM}}^2 + \chi\,(\boldsymbol{B}\times\boldsymbol{\mu}^s) = 0\,, \tag{38}$$

where $\boldsymbol{\mu}^s = (\mu_x^s, \mu_y^s, \mu_z^s)$ denotes the spin accumulation and ℓ_{NM} is the spin diffusion length in the normal metal. The parameter $\chi = g\mu_B/D$ depends on the effective gyromagnetic factor g, the Bohr magneton μ_B, and the diffusion constant D of the normal metal.

The spin injected from the altermagnet is polarized along the Néel vector $\boldsymbol{N}$ of the AM,

$$\boldsymbol{\mu}^s_{\rm AM} = \mu^s_{\rm AM}\,\boldsymbol{N}\,. \tag{39}$$

Here $\mu^s_{\rm AM}$ is the spin accumulation at the edges of the AM strip induced by the charge current in the AM, and given by Eq. (22). Spin injection across the AM/NM interface is described by the boundary condition

$$-\hat{\boldsymbol{n}}\cdot\boldsymbol{j}_s = G_B\,(\mu^s_{\rm AM} - \mu^s)\Big|_{x=0}\,, \tag{40}$$

where G_B denotes the interface spin conductance.

Solving the diffusion equation with the boundary condition above yields the spin accumulation in the NM,

$$\begin{aligned}\boldsymbol{\mu}_s(x) = \frac{G_B}{G_B+\sigma_N\alpha}\,\mu_s^{\rm AM}\Big[&(\boldsymbol{N}\cdot\hat{\boldsymbol{B}})\hat{\boldsymbol{B}}\,e^{-x/\ell_{NM}}\\ &+\boldsymbol{N}\times\hat{\boldsymbol{B}}\,e^{-\alpha x}\sin(\beta x)\\ &+\hat{\boldsymbol{B}}\times(\boldsymbol{N}\times\hat{\boldsymbol{B}})\,e^{-\alpha x}\cos(\beta x)\Big]\,,\end{aligned} \tag{41}$$

where $\hat{\boldsymbol{B}} = \boldsymbol{B}/|\boldsymbol{B}|$, σ_N is the conductivity of the normal metal, and α (β) is the real (imaginary) part of $\sqrt{1/\ell_{NM}^2 + i\chi B}$.

A ferromagnetic detector placed at position $x = L$ measures the non-local voltage [42, 43]:

$$V_{NL}(\boldsymbol{m}) = V_0 + P\,\boldsymbol{\mu}_s(L)\cdot\boldsymbol{m}\,, \tag{42}$$

where V_0 is a spin-independent voltage, and P is the polarization of the F detector whose polarization is parallel to the unit vector $\boldsymbol{m}$.

The relevant observable is the voltage difference, $\Delta V_{NL} \equiv V(\hat{\boldsymbol{m}}) - V(-\hat{\boldsymbol{m}})$, measured for opposite orientations of the detector magnetization. From Eqs. (41) and (42) we obtain:

$$\begin{aligned}\Delta V_{NL} = \frac{2P\,G_B\mu^s_{\rm AM}}{(G_B+\sigma_N\alpha)}\,\hat{\boldsymbol{m}}\cdot\Big[&(\boldsymbol{N}\cdot\hat{\boldsymbol{B}})\hat{\boldsymbol{B}}\,e^{-L/\ell_{NM}}\\ &+\boldsymbol{N}\times\hat{\boldsymbol{B}}\,e^{-\alpha L}\sin(\beta L)\\ &+\hat{\boldsymbol{B}}\times(\boldsymbol{N}\times\hat{\boldsymbol{B}})\,e^{-\alpha L}\cos(\beta L)\Big]\,.\end{aligned} \tag{43}$$

Let us first analyze the case of a zero Hanle field. After substitution of Eq. (22) for $\mu_s^{\rm AM}$ we obtain:

$$\Delta V_{NL} = \frac{2P\,G_B}{(G_B+\sigma_N\alpha)}\,E_y T_{xy}\ell_s\,\hat{\boldsymbol{m}}\cdot\boldsymbol{N}e^{-L/\ell_{NM}}\ . \quad (44)$$

Thus, the non-local voltage is proportional to the altermagnetic tensor T_{xy} and maximized when the Néel vector of the AM is collinear to the magnetization of the FM.

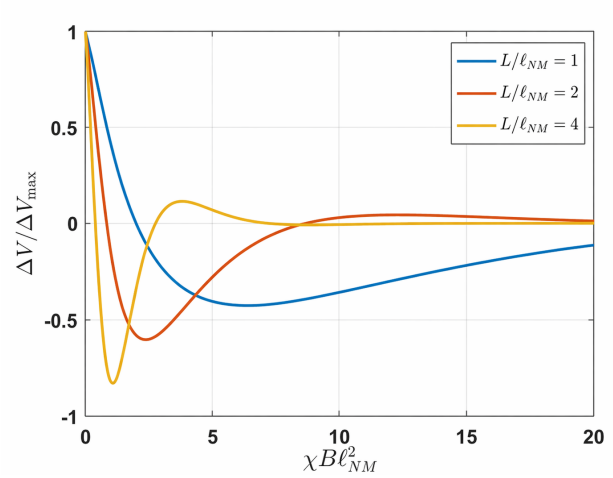

Figure 7. Normalized nonlocal voltage $\Delta V/\Delta V_{\rm max}$ as a function of $\chi B\ell_{NM}^2$ for different injector–detector separations $L/\ell_{NM} = 1, 2, 4$. The curves are obtained from the general expression for the nonlocal signal, evaluated for a magnetic field applied along the z direction and a detector magnetization oriented along the y axis. The Néel vector is chosen in the plane perpendicular to the field, with components $N_x = \cos\theta$ and $N_y = \sin\theta$, using $\theta = \pi/4$. The simulation is performed in dimensionless units with $\ell_{NM} = 1$, so that the magnetic field dependence enters exclusively through the combination $\chi B\ell_{NM}^2$.

For a finite field, we consider as an illustrative example an external magnetic field applied along the z axis, $\boldsymbol{B} = B\hat{z}$, while the magnetization of the ferromagnetic detector is oriented along the transverse y direction, $\boldsymbol{m} = \hat{y}$. In this case, we obtain

$$\Delta V_{NL} = \frac{2P\,G_B\mu_{\rm AM}^s}{(G_B+\sigma_N\alpha)}\ e^{-\alpha L}\Big[N_x\,\sin(\beta L) + N_y\,\cos(\beta L)\Big]\ . \quad (45)$$

Figure 7 shows the corresponding nonlocal Hanle curves obtained from Eq. (45) for this particular geometry, highlighting the precession and dephasing of the spin accumulation generated by the altermagnet as the magnetic field is varied, for different injector–detector separations.

VI. CONCLUSIONS

Building on a kinetic-equation approach, we formulate coupled drift–diffusion equations to describe charge and spin transport in hybrid devices containing altermagnetic materials.

We first analyze the spin-splitter effect, namely the conversion of charge currents into spin currents, in diffusive altermagnetic strips for several device geometries. We then investigate the reciprocal phenomenon—the inverse spin-splitter effect—where an injected spin accumulation generates a transverse electrical response in the altermagnet. For both extended and localized spin injection, we derive closed-form expressions for the induced voltage in the weak-coupling regime and validate them through numerical solutions of the coupled diffusion equations.

Motivated by a recent experiment, we also apply our theoretical framework to hybrid multiterminal geometries in which an altermagnetic strip acts as a spin injector for a diffusive normal metal. We demonstrate that the spin accumulation generated by the spin-splitter effect in the altermagnet and injected in to the normal wire, can be efficiently detected using a conventional ferromagnetic electrode in a nonlocal configuration. The measured nonlocal voltage is proportional to the scalar product of the Néel vector of the altermagnet and the polarization of the ferromagnetic detector.

Finally, we analyze the effect of an external magnetic field in the same geometry. The resulting Hanle-type signal exhibits the characteristic oscillatory behavior associated with spin precession during diffusive transport, providing another direct electrical probe of spin injection from altermagnets.

Our theory establishes altermagnets as robust and electrically controllable sources of spin in multiterminal spintronic devices and can be straightforwardly adapted to a wide variety of hybrid structures combining altermagnets, normal metals, and ferromagnets.

ACKNOWLEDGEMENTS

We thank I. V. Tokatly, F. Casanova and M. Borra for useful discussions and support in this work. N.S. and G.D.P. acknowledge support from the Programa de Desarrollo de las Ciencias Básicas (PEDECIBA) and from the grant number FCE-3-2024-1-180709 of the Agencia Nacional de Investigación e Innovación (Uruguay). The work of T.K. was supported by the Research Council of Finland through DYNCOR, Project Number 354735 and through the Finnish Quantum Flagship, Project Number 359240. His work is part of the Finnish Centre of Excellence in Quantum Materials (QMAT). F.S.B. acknowledges financial support from the Spanish MCIN/AEI/10.13039/501100011033 through grant PID2023-148225NB-C31; from the European Union's Horizon Europe programme through grant

JOSEPHINE (No. 101130224); and from the Carolina Foundation, at the early stage of this project, through its cooperation with the CSIC (reference CAROL24026).

Appendix A: Derivation of the inverse spin–splitter voltage for point-like spin injection

In this Appendix we outline the derivation of Eq. (36), for the average spin accumulation in the setup, its expansion to first order in $G_B W/\sigma$, Eq. (37), and Eq. (35) for the inverse spin–splitter voltage $V_{\rm ISS}$ induced by a localized spin injection at the boundary of a finite altermagnetic strip.

We consider a two-dimensional altermagnet occupying the region $x \in [-\frac{L_x}{2}, \frac{L_x}{2}]$ and $y \in [-\frac{L_y}{2}, \frac{L_y}{2}]$. To leading order in the spin–momentum coupling T_{xy}, charge and spin potentials obey the kinetic diffusion equations, Eqs. (12,13) in the main text, which read

$$(\partial_x^2 + \partial_y^2)\mu + 2T_{xy}\partial_x\partial_y\mu^s = 0 \,, \tag{A1}$$

$$(\partial_x^2 + \partial_y^2)\mu^s + 2T_{xy}\partial_x\partial_y\mu = \frac{\mu^s}{\ell_s^2} \,, \tag{A2}$$

where $\ell_s = \sqrt{D\tau_s}$ is the spin relaxation length.

Spin is injected locally at the upper boundary $y = \frac{L_y}{2}$ through a narrow contact of width $W \ll \ell_s, L_{x,y}$, which we approximate using a δ-function. The boundary conditions, Eqs. (33,32,34), for the spin sector read

$$\partial_y\mu^s(x, -\frac{L_y}{2}) + T_{xy}\partial_x\mu = 0 \,, \tag{A3}$$

$$\sigma_D(\partial_y\mu^s(x, \frac{L_y}{2}) + T_{xy}\partial_x\mu) = 2G_B W\,\delta(x)\,[V_s - \mu^s(x, \frac{L_y}{2})] \,, \tag{A4}$$

$$\partial_x\mu^s(\pm\frac{L_x}{2}, y) + T_{xy}\partial_y\mu = 0 \,. \tag{A5}$$

Charge currents vanish at all boundaries, that is,

$$\partial_x\mu(\pm\frac{L_x}{2}, y) = 0 \,, \tag{A6}$$

$$\partial_y\mu(x, \pm\frac{L_y}{2}) = 0 \,. \tag{A7}$$

1. Spatially averaged spin accumulation

We treat the system perturbatively in T_{xy}. First, we consider only μ^s and derive Eq. (36). To first order in T_{xy}, Eqs. (A2-A5) read

$$(\partial_{xx} + \partial_{yy})\mu^s = \frac{1}{\ell_s^2}\mu^s \,, \tag{A8}$$

$$\partial_y\mu^s(x, -\frac{L_y}{2}) = 0 \,, \tag{A9}$$

$$\sigma_D(\partial_y\mu^s(x, \frac{L_y}{2})) = 2G_B\,W\delta(x)\,[V_s - \mu^s(x, \frac{L_y}{2})] \,, \tag{A10}$$

$$\partial_x\mu^s(\pm\frac{L_x}{2}, y) = 0 \,, \tag{A11}$$

because μ is already proportional to T_{xy} as seen from Eq. (A1). The spatially averaged spin accumulation is defined as

$$\langle\mu^s\rangle = \frac{1}{L_x L_y}\int_{-\frac{L_x}{2}}^{\frac{L_x}{2}} dx \int_{-\frac{L_y}{2}}^{\frac{L_y}{2}} dy\; \mu^s(x,y) \,. \tag{A12}$$

Exploiting Eqs. (A8–A11) and applying Gauss' theorem, we find

$$\begin{aligned}\langle\mu^s\rangle &= \frac{\ell_s^2}{L_x L_y}\int_{-\frac{L_x}{2}}^{\frac{L_x}{2}} dx \int_{-\frac{L_y}{2}}^{\frac{L_y}{2}} dy\; (\partial_{xx} + \partial_{yy})\mu^s(x,y) \\ &= \frac{\ell_s^2}{L_x L_y}\int_{\rm edges} dl n_k \partial_k\mu^s \\ &= \frac{\ell_s^2}{L_x L_y}\int_{-\frac{L_x}{2}}^{\frac{L_x}{2}} dx 2\frac{G_B}{\sigma_D} W\delta(x)[V_s - \mu^s(x, \frac{L_y}{2})] \\ &= \frac{2G_B W\,\ell_s^2}{\sigma_D L_x L_y}\left[V_s - \mu^s(0, \frac{L_y}{2})\right] \,. \end{aligned} \tag{A13}$$

This corresponds to Eq. (36) in the main text.

Next, we consider its weak-coupling limit and derive Eq. (37) in the main text. In the weak-coupling limit $G_B \ll \sigma_D/\ell_s$, the spin accumulation at the injection point $\mu^s(0, \frac{L_y}{2})$ contributes only at order $\mathcal{O}\Big(\left(\frac{G_B\ell_s}{\sigma_D}\right)^2\Big)$ and can therefore be neglected at leading order. This yields

$$\langle\mu^s\rangle \simeq \frac{2G_B W\,\ell_s^2}{\sigma_D L_x L_y}\,V_s \,. \tag{A14}$$

This corresponds to Eq. (37) in the main text.

2. Inverse spin–splitter voltage

Next, we consider the electrochemical potential μ and use it to derive Eq. (35). To first order in T_{xy}, μ is spatially constant in the absence of injected charge currents. At this order, μ satisfies Eqs. (A1, A6, A7), with the spin accumulation μ^s evaluated at first order in T_{xy}.

The inverse spin–splitter voltage is defined as the voltage drop along the transverse x-direction, averaged

over the longitudinal direction y,

$$V_{\rm ISS} = \frac{1}{L_y}\int_{-\frac{L_x}{2}}^{\frac{L_x}{2}} dx \int_{-\frac{L_y}{2}}^{\frac{L_y}{2}} dy\, \partial_x \mu(x,y)\ . \tag{A15}$$

To obtain a closed expression for $V_{\rm ISS}$, we exploit current conservation. In the steady state, the charge current density satisfies $\partial_k j_k = 0$. Since no charge current enters or leaves the system, the charge current integrated over the y-direction must vanish, yielding

$$0 = \int_{-\frac{L_y}{2}}^{\frac{L_y}{2}} dy\, \left(\partial_x \mu + T_{xy}\partial_y \mu^s\right)\ . \tag{A16}$$

The second term can be evaluated explicitly, leading to

$$\partial_x \int_{-\frac{L_y}{2}}^{\frac{L_y}{2}} dy\, \mu(x,y) = -\,T_{xy}\left[\mu^s(x,\tfrac{L_y}{2}) - \mu^s(x,-\tfrac{L_y}{2})\right]\ . \tag{A17}$$

A further integration over x then yields

$$V_{\rm ISS} = -\,\frac{T_{xy}}{L_y}\int_{-\frac{L_x}{2}}^{\frac{L_x}{2}} dx\, \left[\mu^s(x,\tfrac{L_y}{2}) - \mu^s(x,-\tfrac{L_y}{2})\right]\ . \tag{A18}$$

To proceed, it is convenient to express Eq. (A18) in terms of the spin accumulation integrated along the transverse direction. We therefore define

$$I_x(y) \equiv \int_{-\frac{L_x}{2}}^{\frac{L_x}{2}} dx\, \mu^s(x,y)\ . \tag{A19}$$

In terms of $I_x(y)$, Eq. (A18) becomes

$$V_{\rm ISS} = -\,\frac{T_{xy}}{L_y}\left[I_x\left(\tfrac{L_y}{2}\right) - I_x\left(-\tfrac{L_y}{2}\right)\right]\ . \tag{A20}$$

The spin accumulation μ^s obeys the diffusion equation Eq. A8.

Integrating this equation over $x \in [-L_x/2, L_x/2]$ and using the boundary conditions of vanishing spin current at $x = \pm L_x/2$, one finds that $I_x(y)$ satisfies the effective one–dimensional equation

$$\partial_{yy} I_x(y) = \frac{I_x(y)}{\ell_s^2}\ . \tag{A21}$$

The general solution of Eq. (A21) reads

$$I_x(y) = A\cosh\left(\frac{y+\frac{L_y}{2}}{\ell_s}\right) + B\sinh\left(\frac{y+\frac{L_y}{2}}{\ell_s}\right)\ , \tag{A22}$$

where A and B are constants fixed by the boundary conditions in the y-direction. At the lower boundary $y = -L_y/2$, no spin current is injected, implying

$$\partial_y I_x\left(-\tfrac{L_y}{2}\right) = 0\ . \tag{A23}$$

This implies $B = 0$. At the upper boundary $y = +L_y/2$, the point-like spin injector leads to

$$\partial_y I_x\left(\tfrac{L_y}{2}\right) = \frac{2G_B W}{\sigma_D}\left[V_s - \mu^s(0,\tfrac{L_y}{2})\right]\ . \tag{A24}$$

Thus,

$$A = \frac{1}{\sinh\left(\frac{L_y}{\ell_s}\right)}\frac{2G_B W\ell_s}{\sigma_D}\left[V_s - \mu^s(0,\tfrac{L_y}{2})\right]\ . \tag{A25}$$

Using the relation between the injected spin accumulation and its spatial average, Eq.(A13),

$$\langle\mu^s\rangle = \frac{2G_B W\,\ell_s^2}{\sigma_D L_x L_y}\left[V_s - \mu^s(0,\tfrac{L_y}{2})\right]\ , \tag{A26}$$

we find

$$A = \frac{1}{\sinh\left(\frac{L_y}{\ell_s}\right)}\frac{L_x L_y}{\ell_s}\langle\mu^s\rangle\ . \tag{A27}$$

Evaluating the solution (A22) at $y = \pm L_y/2$, one finds

$$I_x\left(\tfrac{L_y}{2}\right) - I_x\left(-\tfrac{L_y}{2}\right) = \frac{L_x L_y}{\ell_s}\langle\mu^s\rangle\tanh\left(\frac{L_y}{2\ell_s}\right)\ . \tag{A28}$$

Finally, substituting this result into Eq. (A20), we obtain

$$V_{\rm ISS} = -\,T_{xy}\,\frac{L_x}{\ell_s}\,\langle\mu^s\rangle\,\tanh\left(\frac{L_y}{2\ell_s}\right)\ , \tag{A29}$$

which is Eq. (35) in the main text for the inverse spin–splitter voltage generated by a point-like spin injector.

[1] Libor Šmejkal, Jairo Sinova, and Tomas Jungwirth. Emerging research landscape of altermagnetism. *Phys. Rev. X*, 12:040501, Dec 2022.

[2] Rafael González-Hernández, Libor Šmejkal, Karel

Výborný, Yuta Yahagi, Jairo Sinova, Tomas Jungwirth, and Jakub Železný. Efficient electrical spin splitter based on nonrelativistic collinear antiferromagnetism. *Phys. Rev. Lett.*, 126:127701, Mar 2021.

[3] Sachchidanand Das, Dhavala Suri, and Abhiram Soori. Transport across junctions of altermagnets with normal metals and ferromagnets. *Journal of Physics: Condensed Matter*, 35(43):435302, 2023.

[4] Xian-Peng Zhang, Xiaolong Fan, Xiangrong Wang, and Yugui Yao. Electric readout of the n\'eel vector in an altermagnet. *arXiv preprint arXiv:2409.10088*, 2024.

[5] O Gomonay, VP Kravchuk, R Jaeschke-Ubiergo, KV Yershov, T Jungwirth, L Šmejkal, J van den Brink, and J Sinova. Structure, control, and dynamics of altermagnetic textures. *npj Spintronics*, 2(1):35, 2024.

[6] Kazuki Maeda, Bo Lu, Keiji Yada, and Yukio Tanaka. Theory of tunneling spectroscopy in unconventional p-wave magnet-superconductor hybrid structures. *Journal of the Physical Society of Japan*, 93(11):114703, 2024.

[7] Pavlo Sukhachov and Jacob Linder. Impurity-induced friedel oscillations in altermagnets and p-wave magnets. *Phys. Rev. B*, 110:205114, Nov 2024.

[8] Javier Sivianes, Flaviano José dos Santos, and Julen Ibañez-Azpiroz. Optical signatures of spin symmetries in unconventional magnets. *Physical Review Letters*, 134(19):196907, 2025.

[9] Jian Yang, Zheng-Xin Liu, and Chen Fang. Symmetry invariants and classes of quasiparticles in magnetically ordered systems having weak spin-orbit coupling. *Nature Communications*, 15(1):10203, 2024.

[10] Yu-Xuan Li and Cheng-Cheng Liu. Majorana corner modes and tunable patterns in an altermagnet heterostructure. *Phys. Rev. B*, 108:205410, Nov 2023.

[11] Yu-Xuan Li. Realizing tunable higher-order topological superconductors with altermagnets. *Phys. Rev. B*, 109:224502, Jun 2024.

[12] Ricardo Zarzuela, Rodrigo Jaeschke-Ubiergo, Olena Gomonay, Libor Šmejkal, and Jairo Sinova. Transport theory and spin-transfer physics in d-wave altermagnets. *Physical Review B*, 111(6):064422, 2025.

[13] Cong He, Zhenchao Wen, Jun Okabayashi, Yoshio Miura, Tianyi Ma, Tadakatsu Ohkubo, Takeshi Seki, Hiroaki Sukegawa, and Seiji Mitani. Evidence for single variant in altermagnetic RuO_2 (101) thin films. *Nature Communications*, 16(1):8235, 2025.

[14] Sonka Reimers, Lukas Odenbreit, Libor Šmejkal, Vladimir N Strocov, Procopios Constantinou, Anna B Hellenes, Rodrigo Jaeschke Ubiergo, Warlley H Campos, Venkata K Bharadwaj, Atasi Chakraborty, et al. Direct observation of altermagnetic band splitting in crsb thin films. *Nature Communications*, 15(1):2116, 2024.

[15] Olena Fedchenko, Jan Minár, Akashdeep Akashdeep, Sunil Wilfred D'Souza, Dmitry Vasilyev, Olena Tkach, Lukas Odenbreit, Quynh Nguyen, Dmytro Kutnyakhov, Nils Wind, et al. Observation of time-reversal symmetry breaking in the band structure of altermagnetic RuO_2. *Science advances*, 10(5):eadj4883, 2024.

[16] Yaqin Guo, Jing Zhang, Zengtai Zhu, Yuan-yuan Jiang, Longxing Jiang, Chuangwen Wu, Jing Dong, Xing Xu, Wenqing He, Bin He, et al. Direct and inverse spin splitting effects in altermagnetic RuO_2. *Advanced Science*, page 2400967, 2024.

[17] Hongyu Chen, Zi-An Wang, Peixin Qin, Ziang Meng, Xiaorong Zhou, Xiaoning Wang, Li Liu, Guojian Zhao, Zhiyuan Duan, Tianli Zhang, et al. Spin-splitting magnetoresistance in altermagnetic RuO_2 thin films. *Advanced Materials*, 37(34):2507764, 2025.

[18] Yu-Xin Li, Yiyuan Chen, Liqing Pan, Shuai Li, Song-Bo Zhang, and Hai-Zhou Lu. Exploration of altermagnetism in RuO_2. *arXiv preprint arXiv:2509.19932*, 2025.

[19] Fangqi Liu, Zhenhua Zhang, Xiaojuan Yuan, Yong Liu, Sicong Zhu, Zhihong Lu, and Rui Xiong. Giant tunneling magnetoresistance in insulated altermagnet/ferromagnet junctions induced by spin-dependent tunneling effect. *Phys. Rev. B*, 110:134437, Oct 2024.

[20] Bo Lu, Kazuki Maeda, Hiroyuki Ito, Keiji Yada, and Yukio Tanaka. φ josephson junction induced by altermagnetism. *Phys. Rev. Lett.*, 133:226002, Nov 2024.

[21] Tim Kokkeler, Ilya Tokatly, and F. Sebastian Bergeret. Quantum transport theory for unconventional magnets: Interplay of altermagnetism and p-wave magnetism with superconductivity. *SciPost Physics*, 18(6):178, 2025.

[22] Rodrigo de las Heras, Tim Kokkeler, Stefan Ilić, Ilya V Tokatly, and F Sebastian Bergeret. Interplay between superconductivity and altermagnetism in disordered materials and heterostructures. *arXiv preprint arXiv:2512.04819*, 2025.

[23] Debashish Mondal, Amartya Pal, Arijit Saha, and Tanay Nag. Distinguishing between topological majorana and trivial zero modes via transport and shot noise study in an altermagnet heterostructure. *arXiv preprint arXiv:2409.08009*, 2024.

[24] Miina Leiviskä, Javier Rial, Antonín Bad'ura, Rafael Lopes Seeger, Ismaïla Kounta, Sebastian Beckert, Dominik Kriegner, Isabelle Joumard, Eva Schmoranzerová, Jairo Sinova, Olena Gomonay, Andy Thomas, Sebastian T. B. Goennenwein, Helena Reichlová, Libor Šmejkal, Lisa Michez, Tomá š Jungwirth, and Vincent Baltz. Anisotropy of the anomalous hall effect in thin films of the altermagnet candidate mn_5si_3. *Phys. Rev. B*, 109:224430, Jun 2024.

[25] Qiang Cheng, Yue Mao, and Qing-Feng Sun. Field-free josephson diode effect in altermagnet/normal metal/altermagnet junctions. *Phys. Rev. B*, 110:014518, Jul 2024.

[26] Yuri Fukaya, Bo Lu, Keiji Yada, Yukio Tanaka, and Jorge Cayao. Superconducting phenomena in systems with unconventional magnets. *arXiv preprint arXiv:2502.15400*, 2025.

[27] Chi Sun, Arne Brataas, and Jacob Linder. Andreev reflection in altermagnets. *Physical Review B*, 108(5):054511, 2023.

[28] Hans Gløckner Giil and Jacob Linder. Superconductor-altermagnet memory functionality without stray fields. *Physical Review B*, 109(13):134511, 2024.

[29] Debika Debnath, Arijit Saha, and Paramita Dutta. Spin-polarization and diode effect in thermoelectric current through altermagnet-based superconductor heterostructures. *arXiv*, abs/2509.12198, Sep 2025.

[30] Tomas Jungwirth, Rafael M Fernandes, Jairo Sinova, and Libor Smejkal. Altermagnets and beyond: Nodal magnetically-ordered phases. *arXiv preprint arXiv:2409.10034*, 2024.

[31] Ling Bai, Wanxiang Feng, Siyuan Liu, Libor Šmejkal, Yuriy Mokrousov, and Yugui Yao. Altermagnetism: Exploring new frontiers in magnetism and spintronics.

Advanced Functional Materials, page 2409327, 2024.

[32] Tomas Jungwirth, J Sinova, P Wadley, D Kriegner, H Reichlova, F Krizek, H Ohno, and L Smejkal. Altermagnetic spintronics. *arXiv preprint arXiv:2508.09748*, 2025.

[33] Karl Bergson Hallberg, Erik Wegner Hodt, and Jacob Linder. Visualization of the spin-splitter effect in altermagnets via non-equilibrium green functions on a lattice. *Phys. Rev. B*, 111:174431, May 2025.

[34] Arsen Herasymchuk, Karl Bergson Hallberg, Erik Wegner Hodt, Jacob Linder, E. V. Gorbar, and Pavlo Sukhachov. Electric and spin current vortices in altermagnets. *Phys. Rev. B*, 112:L220404, Dec 2025.

[35] Jone Mencos, Antonin Badura, Eoin Dolan, Sebastian Beckert, Rafael Gonzalez-Hernandez, Ismaila Kounta, Matthieu Petit, Charles Guillemard, Anna Birk Hellenes, Warlley Campos, et al. Direct demonstration of time-reversal-symmetry-breaking spin injection from a compensated magnet. *arXiv preprint arXiv:2512.17427*, 2025.

[36] Xian-Peng Zhang, F Sebastian Bergeret, and Vitaly N Golovach. Theory of spin hall magnetoresistance from a microscopic perspective. *Nano letters*, 19(9):6330–6337, 2019.

[37] Maria B. Lifshits and Michel I. Dyakonov. Swapping spin currents: Interchanging spin and flow directions. *Phys. Rev. Lett.*, 103:186601, Oct 2009.

[38] Miina Leiviskä, Reza Firouzmandi, Kyo-Hoon Ahn, Peter Kubaščik, Zbynek Soban, Satya Prakash Bommanaboyena, Christoph Müller, Dominik Kriegner, Sebastian Sailler, Denise Reustlen, et al. Spin hall magnetoresistance at the altermagnetic insulator/pt interface. *Physical Review Materials*, 9(8):084403, 2025.

[39] Friso Jacobus Jedema, AT Filip, and BJ Van Wees. Electrical spin injection and accumulation at room temperature in an all-metal mesoscopic spin valve. *Nature*, 410(6826):345–348, 2001.

[40] Estitxu Villamor, Miren Isasa, Saül Vélez, Amilcar Bedoya-Pinto, Paolo Vavassori, Luis E Hueso, F Sebastián Bergeret, and Felix Casanova. Modulation of pure spin currents with a ferromagnetic insulator. *Physical Review B*, 91(2):020403, 2015.

[41] Y Ji, A Hoffmann, JS Jiang, JE Pearson, and SD Bader. Non-local spin injection in lateral spin valves. *Journal of Physics D: Applied Physics*, 40(5):1280, 2007.

[42] FJ Jedema, HB Heersche, AT Filip, JJA Baselmans, and BJ Van Wees. Electrical detection of spin precession in a metallic mesoscopic spin valve. *Nature*, 416(6882):713–716, 2002.

[43] Tero T Heikkilä, Mikhail Silaev, Pauli Virtanen, and F Sebastian Bergeret. Thermal, electric and spin transport in superconductor/ferromagnetic-insulator structures. *Progress in Surface Science*, 94(3):100540, 2019.